Supplementary Material to the Article: A Joint Space-Time Probabilistic Model for Agricultural Droughts, Hydrological Droughts and Fire Weather in France.

B. Renard[1], R. Barbero[1], I. Goukouni[1], J.-P. Vidal[2], L. Mimeau[2], C. Furusho-Percot[3], I. Garcia-De-Cortazar-Atauri[3], M. Aubry[3], T. Opitz[4], and D. Allard[4]

[1]INRAE, Aix Marseille University, UR RECOVER, Aix-En-Provence, France
[2]INRAE, UR RIVERLY, Lyon, France
[3]INRAE, US Agroclim, Avignon, France
[4]INRAE, Biostatistics and Spatial Processes (BioSP), Avignon, France

March 13, 2026

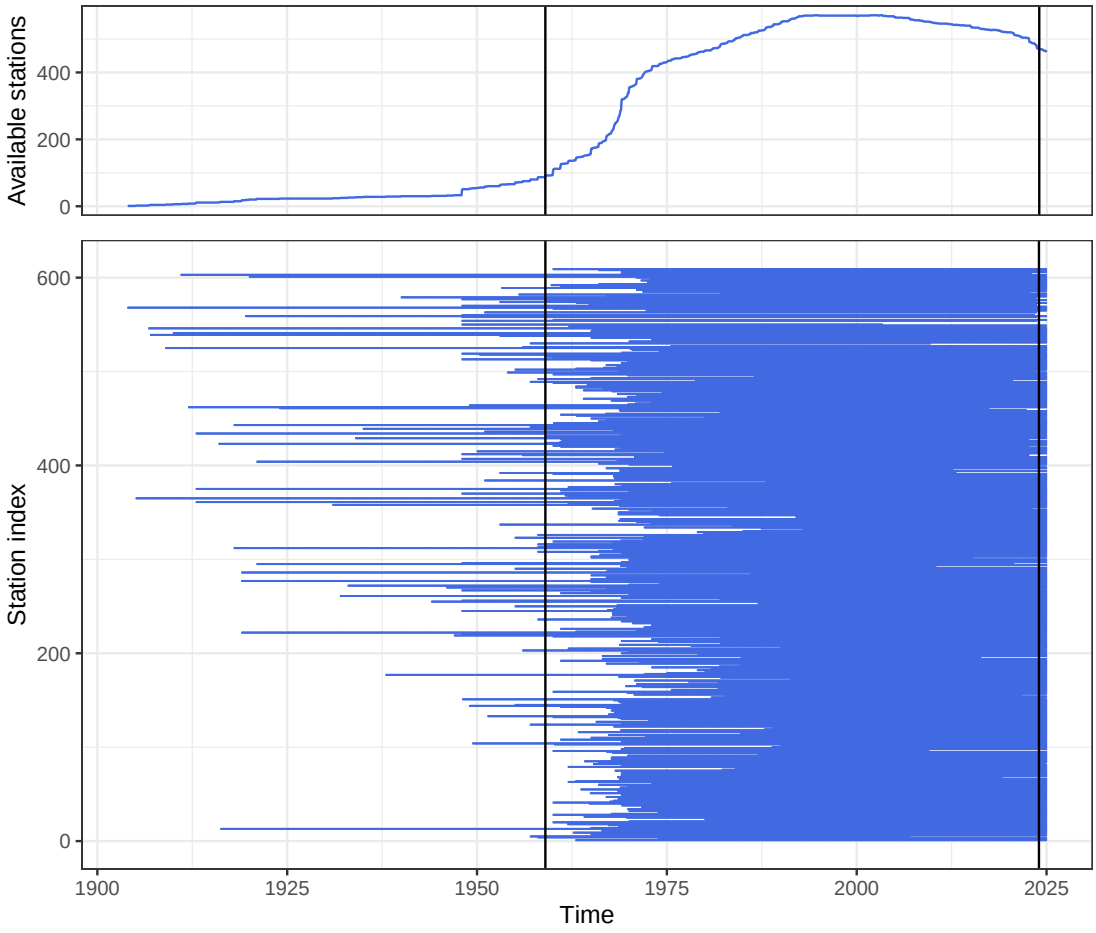

Figure S1: Availability of Q data at hydrometric stations. Vertical lines denote the 1959-2023 period studied in this article.

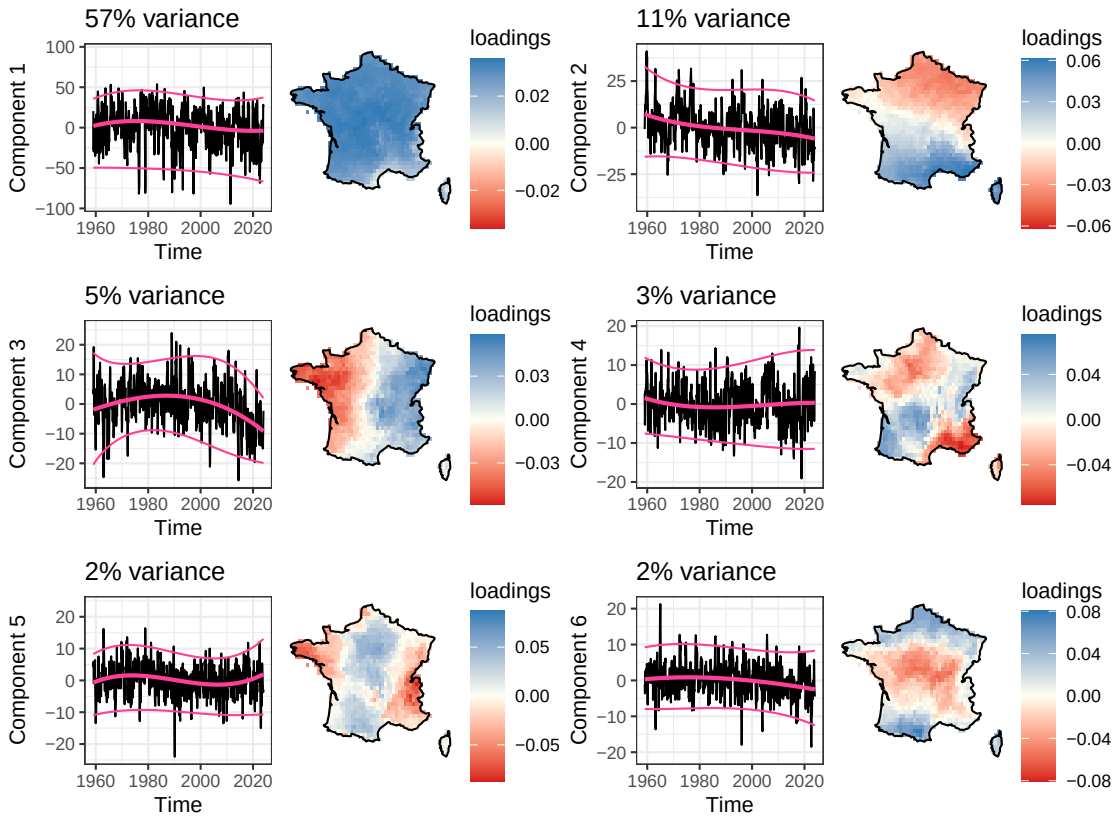

Figure S2: Scores (time series) and loadings (map) associated with the 6 principal components. The thick pink line shows the median of the GAMLSS model fitted to the PC time series, thin lines represent the 95% probability interval.

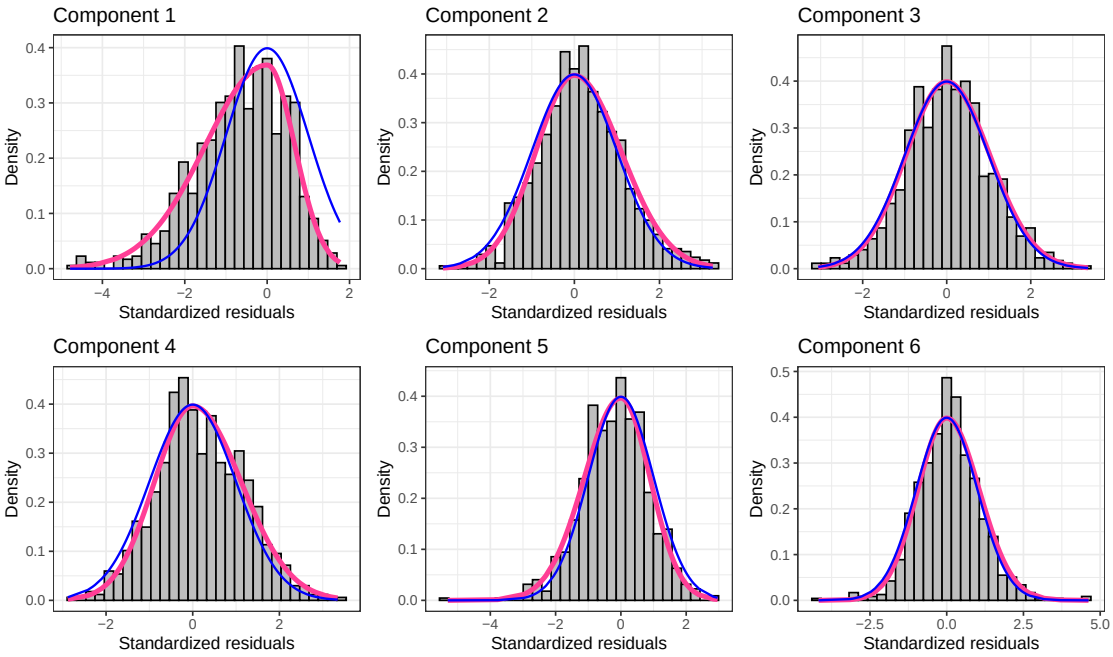

Figure S3: Standardized residuals (histograms) for the principal components GAMLSS model (equation 2), compared with a standard normal density (thin blue) and the estimated skew-normal density (thick pink). On the first component, the skew-normal distribution with constant asymmetry performs well, whereas a bad fit is evident with a normal distribution.

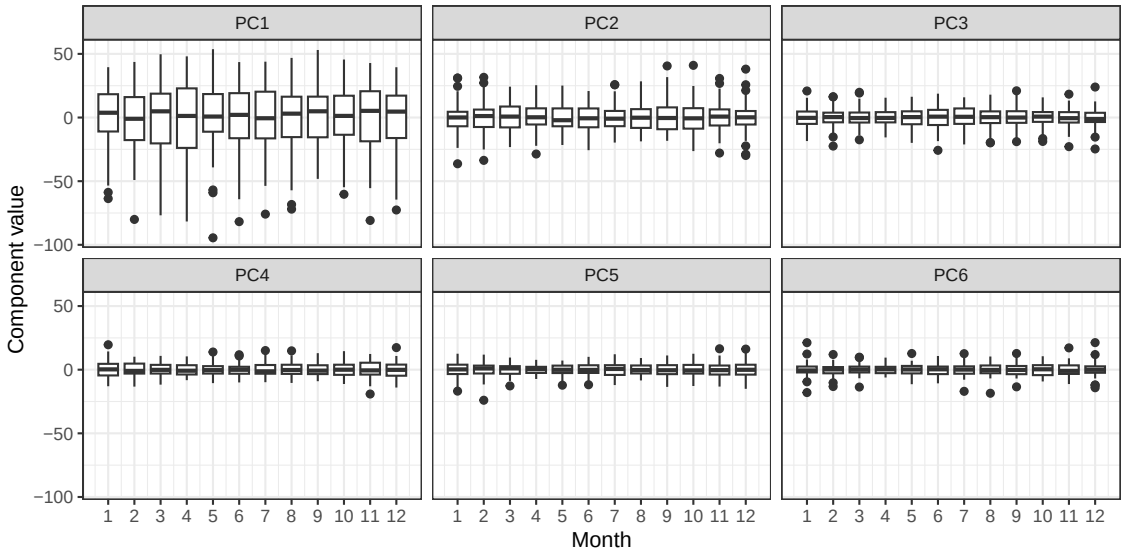

Figure S4: Monthly boxplots of PCA scores associated with the first 6 components, showing the lack of seasonality.

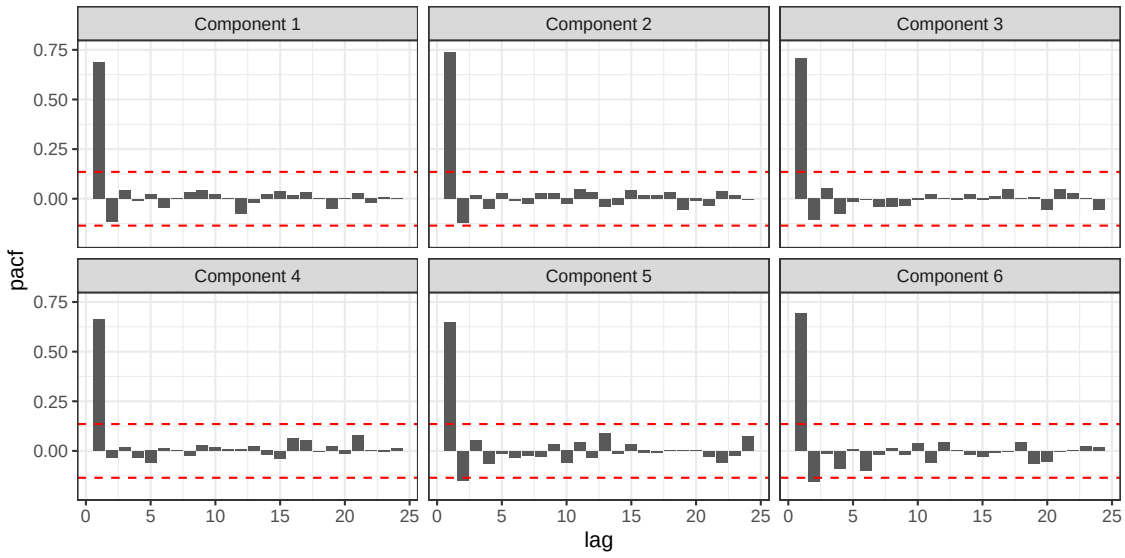

Figure S5: Partial autocorrelation functions associated with the first 6 components. For all components, only the first partial autocorrelation is significant, corresponding to an AR(1) structure.

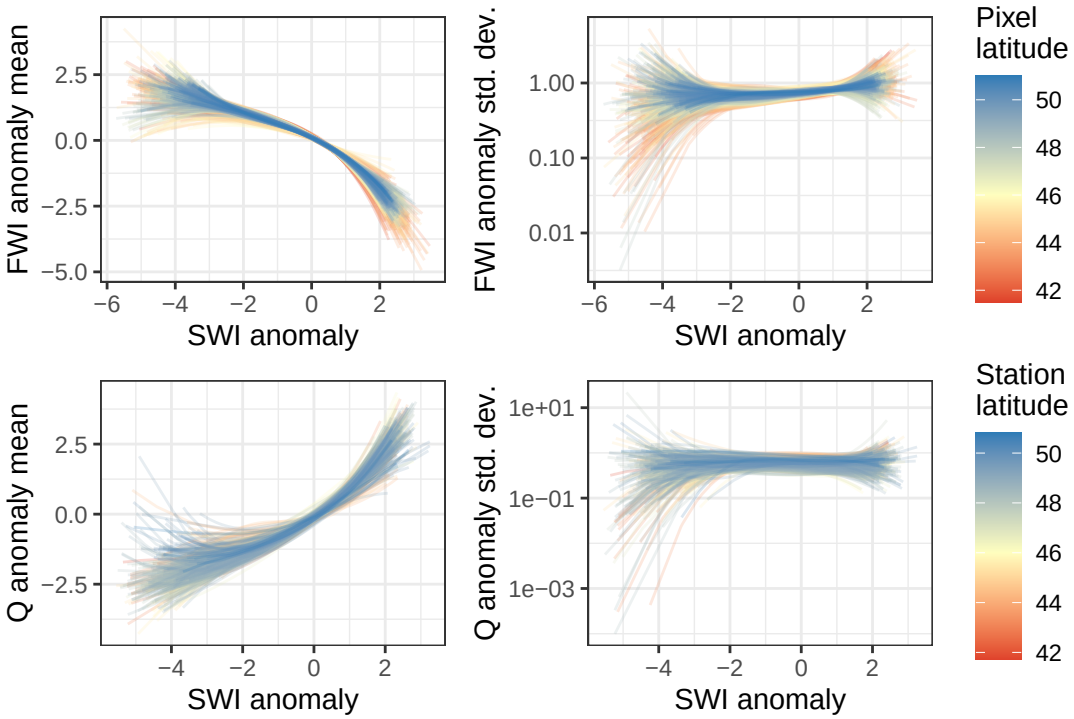

Figure S6: Conditional mean and standard deviation computed from (SWI,FWI) (top) and (SWI,Q) (bottom) GAMLSS models at all pixels /catchments.

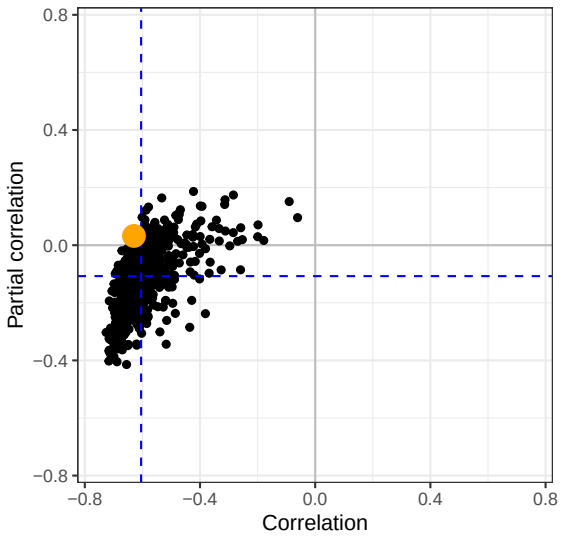

Figure S7: Full vs. partial correlations between FWI and Q at all catchments and nearest pixels. Full correlations are directly computed between FWI and Q anomalies, while partial correlations are computed betweem the residuals of the (SWI,FWI) and (SWI,Q) regressions. Dashed lines represent medians across all catchments.

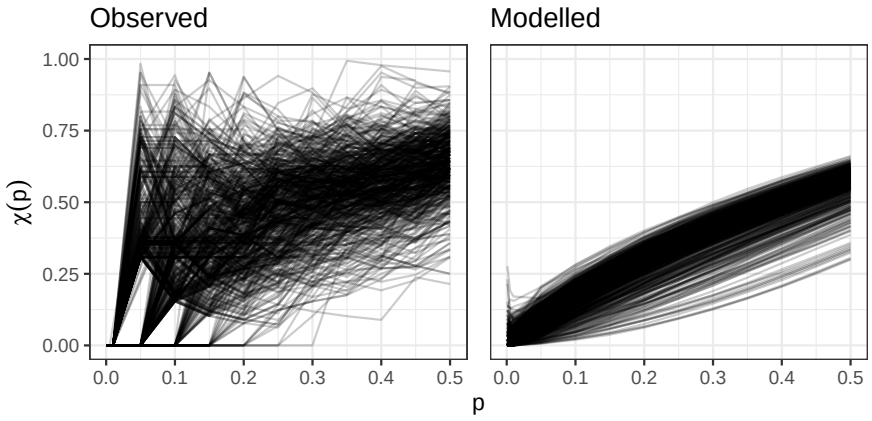

Figure S8: Dependence measure $\chi(p)$ [Coles et al., 1999], corresponding to the frequency (a) or probability (b) of jointly nonexceeding SWI and Q p-quantiles and exceeding FWI $(1-p)$-quantile, divided by p. Each black line corresponds to one station.

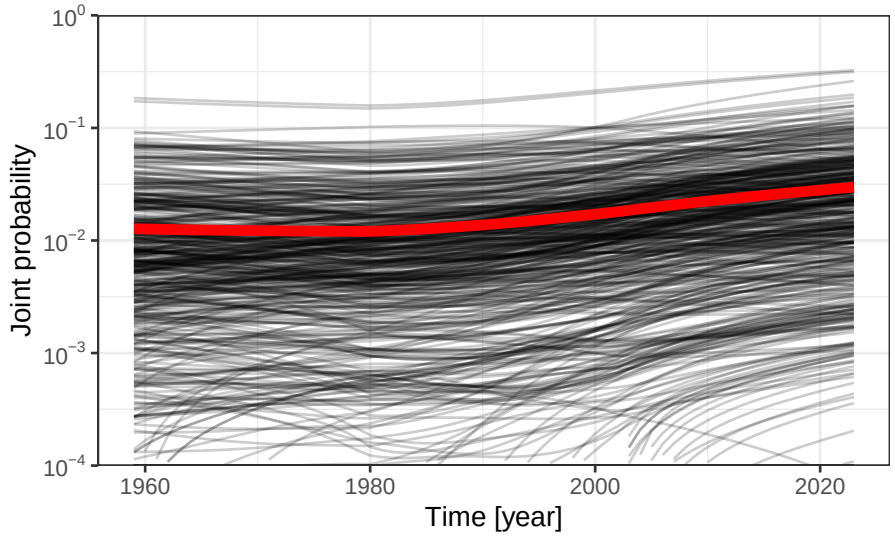

Figure S9: Probability of jointly exceeding the intensity of the 2022 event for all three variables (SWI,FWI,Q) as a function of time. Each individual thin line represents a station, the thick red line is the spatial average.

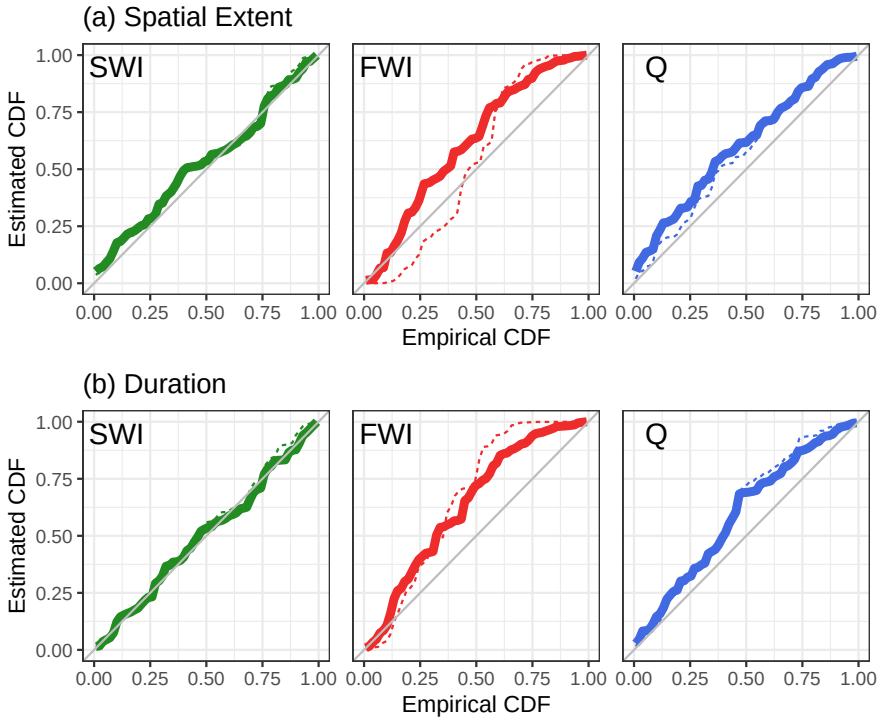

Figure S10: (a) Probability-Probability plot of spatial extents for SWI, FWI and Q. Dotted lines correspond to the model ignoring residual spatial dependence (equation 12 in the paper). The S-shaped dotted red line corresponds to the underestimated variability for FWI when residual dependence is ignored, as discussed in the paper. (b) same as (a) but for durations, defined as the annual number of months during which the 5-year threshold is crossed, averaged over all pixels/stations.

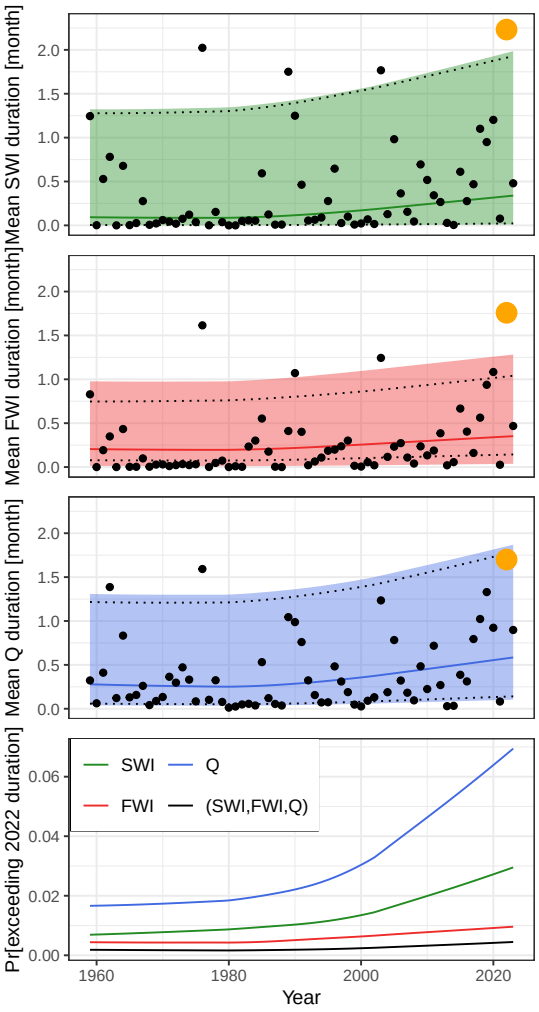

Figure S11: Time-varying distribution of the annual mean duration of SWI, FWI and Q events (top three panels), and time-varying probability of exceeding the duration of the 2022 event for each variable individually and jointly (bottom panel). Points are observations, with the larger golden point highlighting the year 2022. The thick line shows the estimated median, and the filled area extends between the 0.05 and 0.95 quantiles. The dotted lines show the quantiles obtained with a model ignoring residual spatial dependence (equation 12 in the paper).